A Simple Startup Strategy Based on Current Regulation for Back-EMF-Based Sensorless Control of PMSM

Zihui Wang, *Student Member, IEEE*, Kaiyuan Lu, and Frede Blaabjerg, *Fellow, IEEE*

***Abstract*—Back-EMF-based sensorless control of permanent magnet synchronous machines (PMSMs) is preferred in many industrial applications due to its control simplicity and high machine efficiency. Position estimation based on the back-EMF is most reliable in the medium- to high-speed range. For applications where low-speed operation is not required, a simple-structure back-EMF-based sensorless controller coupled with a simple startup procedure offers an attractive low-cost solution. This paper proposes a new startup procedure based on closed-loop current regulation. Compared to the existing methods, the new starting method can work under different load conditions and allows smooth transition from the startup procedure to the back-EMF-based sensorless control mode. In order to determine the successful use of the proposed method in various applications, it stability under different load conditions is discussed in detail. The proposed method is robust when it comes to the motor parameter variation and can be used for both surface-mounted PMSMs (SPMSMs) and interior PMSMs. The method presented in this paper is validated using the experimental results on an SPMSM. A general design guideline is also given.**

***Index Terms*—Back-EMF, current regulation, permanent magnet synchronous machine (PMSM), sensorless control, startup strategy.**

I. Introduction

SENSORLESS control of permanent magnet synchronous machines (PMSMs) has been studied in detail over the last several decades because it reduces system cost. Many high-performance sensorless control methods have been reported, including the method that uses the extended Kalman filter [1], [2], the method based on adaptive observers [3], [4], and the methods based on utilization of multiple current measurements during one switching period [5], or by introducing a special "electrical steady state" to facilitate position estimation [6]. Though it is always interesting to investigate high-performance sensorless control methods, it is worth pointing out that many industrial applications are fan-, pump-, and compressor-type loads [7]. For these applications, high dynamic control performance at low speed during startup is not necessary. Instead, the simplicity and robustness of the control strategy such, as the back-EMF-based method presented in this paper could be more important.

The back-EMF-based method is intended to be operated in medium- to high-speed range; therefore, an additional startup procedure is required. To cover the speed range from zero speed to a medium speed, HF signal injection methods are normally used. The HF voltage component is first injected and then a bandpass filter is used to extract the HF signal from the measured current. This is followed by special signal processing methods to detect the rotor position. At the same time, notch or low-pass filters are needed to extract the fundamental current information for torque and speed control [8]–[10]. As the purpose here is only to start up the drive, it may be too complicated and unnecessary to use HF signal injection methods. The startup issue may also be dealt with by extending the available speed range of the sensorless controller. The idea is that with the speed range extended, the requirement on the startup procedure may be reduced. However, this kind of sensorless controller with the speed range extended requires a special design of the integrator [11]. Even so, it may still suffer from the inaccuracy of the rotor resistance and the inverter nonlinearity effect in the low-speed/low-voltage operation range.

Besides the requirement on the simplicity of the control algorithm, the startup procedure should also be robust and able to work with different load situations to ensure that the drive is able to accelerate to a speed at which the back-EMF is high enough to be accurately sensed. A simple startup method could be to give dc bias currents to the phase windings at the beginning in order to align the rotor to a predetermined position. For applications where it is not possible to rotate the rotor initially, initial rotor position estimation methods based on magnetic saliency may be used, as discussed in [5], [12], and [13]. The motor is then accelerated from standstill to a certain speed by following a ramp frequency or speed command [14], [15]. This is similar to the open-loop *V/f* control used for induction machines. When the *V/f* control is applied to PM machines, due to its open-loop structure with no position or current feedback, the motor may lose its synchronism and the operation may be unstable especially in load conditions. The field-oriented control (FOC) controls the rotor *d*-axis current to be zero for a surface-mounted PMSM (SPMSM), and the *q*-axis current is in proportion to the load torque [16]. An open-loop *V/f* control cannot guarantee that before switching to the FOC, the *d*- and *q*-axes currents are close

Manuscript received January 22, 2011; revised June 9, 2011 and December 24, 2011; accepted January 17, 2012. Date of current version April 20, 2012. Recommended for publication by Associate Editor T. Jahns.

Z. Wang is with the College of Electrical Engineering, Zhejiang University, Hangzhou 310027, China (e-mail: wzh2718@126.com).

K. Lu and F. Blaabjerg are with the Institute of Energy Technology, Aalborg University, Aalborg DK-9220, Denmark (e-mail: klu@et.aau.dk; fbl@et.aau.dk).

Color versions of one or more of the figures in this paper are available online at http://ieeexplore.ieee.org.

Digital Object Identifier 10.1109/TPEL.2012.2186464

to the values that will be generated by the FOC. The absence of current regulation may cause high current and torque ripples during the transition from the startup stage to the FOC stage, which also increases the risk that FOC may not be switched in successfully. To overcome these problems, closed-loop control strategies should be adopted.

In [17] and [18], a so-called *I–f* starting method was proposed. The name of "*I–f*" is mapped from the well-known *V/f* starting method. Instead of specifying a voltage reference used in the *V/f* control, the current in the *I–f* control is specified and maintained constant in a synchronous rotating reference frame. The motor is accelerated by following a ramping up frequency command.

This *I–f* starting method appears to be a better solution to make the startup process smooth and robust, compared to the open-loop *V/f* startup method. An important part in applying this *I–f* starting method is to design a good transition period to allow the sensorless FOC to be smoothly switched in. In [17], a first-order compensator was used to force the position of the synchronous rotating reference frame to approach the rotor position obtained from the back-EMF-based sensorless method. A successful convergence of these two positions depends heavily on the compensator parameters, which is hard to pretun for different drive systems. Similarly in [18], a speed-dependent weight was introduced to rotate the synchronous rotating reference frame to the desired position. In this method, similar to the first-order compensator, it is not easy to find the proper parameters that will secure a successful convergence. Further detailed analysis of the *I–f* method was lacking in [18] with respect to stability issues and general design guidelines.

In this paper, a detailed analysis is given for the *I–f* starting method. A new, simple startup strategy is introduced to allow a smooth torque and speed transition from the startup stage to the sensorless FOC stage. The method proposed in this paper is robust and can work with different load situations. The performance of this startup process is also robust under different motor parameter variations. This paper emphacizes stability which is an essential element to the development of good design guidelines for the *I–f* starting method for various applications. The proposed simple but robust startup method is suitable for applications of pump-, fan-, or compressor-type loads, where low-speed operation is not desired. It offers advantages especially for heating or cooling compressor-type applications, where the load torque is a function of the piston position and during the startup, the change of the load torque requires robust control algorithms.

First, a description of the system topology is given. The new startup strategy is then presented and analyzed. Finally, its performance is validated through experimental results on an SPMSM.

II. Control System for PMSM

The complete control system topology is shown in Fig. 1, which consists of two consecutive procedures: current regulation control for startup and traditional FOC using the position estimated from the back EMF. When the two switches (switches 1 and 2) are connected to terminal 2, the control system presented in Fig. 1 is the traditional FOC of PMSM. The controller is realized in the rotating *d*-, *q*-reference frame. It consists of inner current control loops using proportional–integral (PI) controllers and an outer speed control loop.

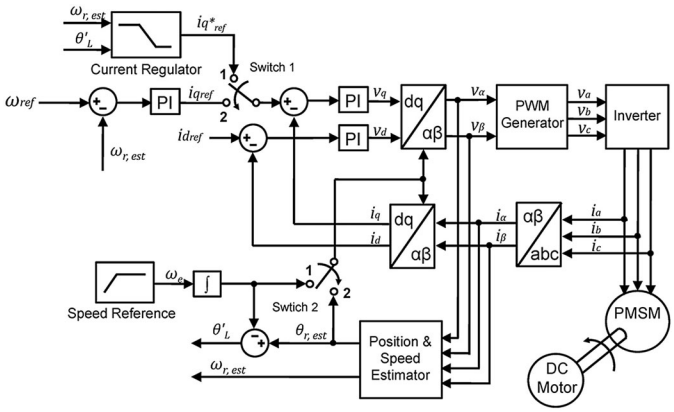

Fig. 1. Vector control scheme with startup procedure for PMSM.

A simple back-EMF-based sensorless control algorithm is used to estimate the position information needed to transfer the variables from the stationary stator α-, β-reference frame to the rotating rotor *d*-, *q*-reference frame. Assuming that the *d*-, *q*-axes inductances are equal, the model of the PMSM may be represented in the α-, β-reference frame as follows:

$$\begin{bmatrix} v_\alpha \\ v_\beta \end{bmatrix} = \begin{bmatrix} R_s & 0 \\ 0 & R_s \end{bmatrix} \begin{bmatrix} i_\alpha \\ i_\beta \end{bmatrix} + \frac{d}{dt} \begin{bmatrix} \psi_\alpha \\ \psi_\beta \end{bmatrix} \tag{1}$$

$$\begin{bmatrix} \psi_\alpha \\ \psi_\beta \end{bmatrix} = \begin{bmatrix} L_1 & 0 \\ 0 & L_1 \end{bmatrix} \begin{bmatrix} i_\alpha \\ i_\beta \end{bmatrix} + \begin{bmatrix} \cos\theta_r \\ \sin\theta_r \end{bmatrix} \psi_{\mathrm{mpm}} \tag{2}$$

where *v*, *i*, and ψ are the stator phase voltage, phase current, and phase total flux linkage, respectively. Subscripts α and β stand for their corresponding α, β components. R_s is the stator phase resistance, θ_r is the rotor angular position in electrical radians, and ψ_{mpm} is the peak value of the rotor PM flux linkage. Inductances L_1 is obtained from the *d*-, *q*-axes inductances (L_d and L_q) as $L_1 \triangleq (L_d + L_q)/2$. By using (1) and (2), the estimated rotor position $\theta_{r,\mathrm{est}}$ and the estimated rotor speed $\omega_{r,\mathrm{est}}$ may be obtained as follows:

$$\psi_\alpha = \int (u_\alpha - R_s \times i_\alpha) dt \tag{3}$$

$$\psi_\beta = \int (u_\beta - R_s \times i_\beta) dt \tag{4}$$

$$\theta_{r,\mathrm{est}} = \tan^{-1} \frac{\psi_\beta - L_1 i_\beta}{\psi_\alpha - L_1 i_\alpha} \tag{5}$$

$$\omega_{r,\mathrm{est}} = \frac{d\,\theta_{r,\mathrm{est}}}{dt}. \tag{6}$$

In practice, the integration of (3), (4) will be affected by the zero-drifting component and it must be compensated, as discussed in, e.g., [19].

This back-EMF-based position estimation algorithm has good performance in the medium- to high-speed range. Working in this speed range, the stator resistance variation and the

nonlinearity of inverter has little influence on the estimated rotor position and may be safely neglected [20]. In the normal operation of the SPMSM, the d-axis current is maintained to be zero, and the q-axis current is regulated to adjust the motor torque. When the motor current is predominant on the q-axis for SPMSMs, the results show that the inductance variation due to the saturation may be neglected [21], [22]. Therefore, with the drift properly compensated in the integration, the back-EMF-based position estimation method (3)–(6) will give satisfactory performance.

In the low-speed range, the back-EMF method suffers from the small magnitude of the back-EMF signal [23]. A separate approach for accelerating the motor from standstill is needed. This is achieved by switching switches 1 and 2 to terminal 1, as shown in Fig. 1. In the starting period, the position information needed in the reference frame transformation is obtained from the integration of a preset speed command. The speed command is first a ramp input. During this period, a constant q-axis current in the synchronous rotating reference frame is applied to accelerate the motor. After a desired speed is reached, the speed command is held constant, and the reference q-axis current is regularly decreased to ensure a smooth transition from the startup procedure to the back-EMF-based FOC method. In this stage, a proper selection of the acceleration rate and the q-axis current decreasing rate is crucial for the motor to avoid losing synchronization, which will be discussed in detail in Section III.

III. Analysis of the Startup Strategy

The proposed startup procedure contains two different stages: a ramp speed reference with a constant q^*-axis current stage and a constant speed reference with a decreasing q-axis current.

A. Ramp Speed Reference With a Constant q-Axis Current

The purpose of this stage is to accelerate the motor from standstill to a desired speed.

During the speed rampup, control is realized in the synchronous rotating reference frame. Its location is obtained by integrating the speed command and is denoted as the d^*q^*-reference frame shown in Fig. 2. The angle between the real rotor dq frame and the synchronous rotating d^*q^*-reference frame is defined as θ_L.

During the speed rampup, the q^*-axis current is maintained constant and the d^*-axis current is set to zero. To start the motor, dc currents are first applied to the motor to align the rotor to the zero position, where the rotor d-axis is aligned with the stator phase-a axis. Then the synchronous rotating reference frame d^*q^* is set to be lagging the real rotor dq frame by 90 electrical degrees, as demonstrated in Fig. 2(a). The q^*-axis current is then aligned to the rotor d-axis and therefore no torque will be generated. The synchronous reference frame d^*q^* will start to rotate due to the integration of the ramp speed command. The angle θ_L will become smaller and correspondingly, the real q-axis current component (i_q) will increase, which is equal to $i_q^* \cos\theta_L$. When the real q-axis current component is large enough to produce a torque that is greater than the load torque, the rotor will start to rotate and the rotor dq-axes will try to follow the rotating synchronous frame d^*q^*-axes, as illustrated in Fig. 2(b).

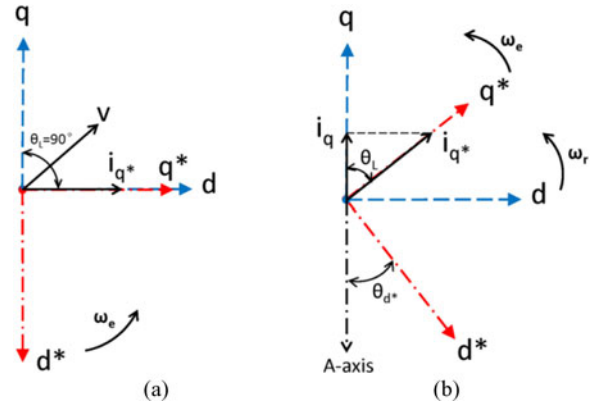

Fig. 2. Phasor diagram in dq and d^*q^* axes in ramp speed operation. (a) Initial situation. (b) During acceleration.

It is important to notice that this *I–f* starting strategy has a self-stabilization capability. The relation between the synchronous frame q^*-axis current i_q^* and the real motor torque T_e is determined by the following:

$$T_e = \frac{3}{2} p i_q^* \cos\theta_L (\psi_{\mathrm{mpm}} + (L_d - L_q) i_q^* \sin\theta_L) \approx K_T i_q^* \cos\theta_L \tag{7}$$

where p is the number of pole pairs of the machine, and K_T is the motor torque constant. The second term of the flux component $(L_d - L_q) i_q^* \sin\theta_L$ could be omitted compared to PM flux ψ_{mpm}. If the acceleration rate is decreased due to the increased load, the rotor speed will decrease and the angle θ_L will become smaller. Referring to Fig. 2(b) and (7), because the q^*-axis current (i_q^*) is kept constant, the real q-axis current component i_q, which is equal to $i_q^* \cos\theta_L$, will then become larger and therefore the machine will generate larger torque to accelerate the rotor and achieve a new balance. Similar self-stabilization mechanism may also be observed when the load torque is decreased.

The self-stabilization mechanism may be lost if angle θ_L is negative which occurs when the synchronous frame q^*-axis is leading the rotor q-axis. In this case, if the load torque is increased, the rotor speed decreases and the angle between the q^*-axis and the q-axis, θ_L, will be enlarged (negative angle). This will cause the electromagnetic torque to decease and therefore the speed of the motor will be further reduced. The rotor speed will then quickly fall to zero. Therefore, it is crucial to keep the synchronous frame q^*-axis always lagging the rotor q-axis and to guarantee that there is enough margin left in the angle θ_L. It may be observed from (7)–(10) that the angle θ_L is determined by the synchronous frame q^*-axis current, the load torque, and the torque component needed to accelerate the rotor. For the same motor output torque, by increasing the synchronous frame q^*-axis current i_q^*, angle θ_L will be increased. Therefore, it is important to have a large enough synchronous frame q^*-axis current, which ensures that the synchronous frame q^*-axis will be lagging the rotor q-axis and there is enough margin left in the angle θ_L to avoid entering the negative θ_L region. For example, if the synchronous frame q^*-axis current is 41% larger than the

rotor real q-axis current, which is the actual current component used for producing torque, the corresponding angle θ_L is 45°.

In this starting period, the speed reference is a ramp function and the rotor is accelerated from standstill. To ensure that the self-stabilization mechanism can be maintained and the acceleration of the rotor can always follow the ramp speed command, it is important to select a proper ramp ratio of the speed reference and this is analyzed next.

The ramp speed reference may be expressed as follows:

$$\omega_e = K_\omega t \tag{8}$$

where ω_e is the electrical angular speed of the rotating synchronous reference frame. It is in proportion to the time t, in a ratio determined by K_ω. In order to find out a proper value for K_ω, it is necessary to consider the following mechanical equation:

$$T_e - T_L = J\frac{d\Omega_r}{dt} = \frac{J}{p}\frac{d\omega_r}{dt} \tag{9}$$

where T_L is the load torque, J is inertia, Ω_r is the mechanical rotor speed, and ω_r is the electrical rotor speed. The motor torque T_e is a function of the angle θ_L, as given in (7). Since θ_L is the angle between the synchronous frame q^*-axis and the rotor q-axis, θ_L will be a function of the time and is determined by the following:

$$\frac{d\theta_L}{dt} = \omega_r - \omega_e. \tag{10}$$

Equations (7)–(10) form a nonlinear system. It may be found that the angle θ_L is actually governed by a second-order, parameter-time dependent, nonlinear differential equation. The load torque may also be speed dependent as for, e.g., a fan load. It is very difficult to analytically solve these equations. But an important assumption may be used here to facilitate the mathematical manipulation. The assumption is based on the fact that during the acceleration, the final rotor speed is not determined by the instantaneous torque, but is determined by the effective average torque accounted in this period. If the average torque is used, the rotor speed at a certain time T may be obtained from (9) as follows:

$$\begin{aligned}\omega_r(T) &= \frac{p}{J}\left(\int_0^T T_e(t)dt - \int_0^T T_L(t)dt\right)\\ &= p\frac{T}{J}(T_{e,\mathrm{ave}} - T_{L,\mathrm{ave}})\end{aligned} \tag{11}$$

where $T_{e,\mathrm{ave}}$ and $T_{L,\mathrm{ave}}$ is the average value of the motor torque $T_e(t)$ and the load torque $T_L(t)$ during the time interval [0,T], respectively. According to (7), since i_q^* is constant, the average motor torque will be corresponding to an average value of angle θ_L as follows:

$$T_{e,\mathrm{ave}} = K_T i_q^* \cos\theta_{L,\mathrm{ave}}. \tag{12}$$

The rotor speed will follow closely to the synchronous rotating speed ω_e. Therefore, it may be assumed that

$$\omega_r(T) = \omega_e(T) = K_\omega T. \tag{13}$$

By substituting (12) and (13) into (11), it may be obtained that

$$K_\omega = p\frac{K_T i_q^* \cos\theta_{L,\mathrm{ave}} - T_{L,\mathrm{ave}}}{J}. \tag{14}$$

The torque constant of the machine K_T and the inertia used in (14) may be obtained from the motor data catalog. The inertia may also be found by performing special tests as, e.g., [24]. For many applications with fan- or pump-type loads, the load torque is proportional to the square of the speed. Once the rated torque is known from the nameplate data, the load torque at different speed may be estimated and an average load torque $T_{L,\mathrm{ave}}$ needed in (14) may then be found. In (14), the angle $\theta_{L,\mathrm{ave}}$ may be difficult to estimate, but the margin of K_ω may be constrained to the following:

$$K_\omega < \frac{p(K_T i_q^* - T_{L,\max})}{J} \tag{15}$$

where $T_{L,\max}$ is the maximum load torque the drive may experience during the startup. Equation (15) gives a good design guide of how to properly choose the ratio of the speed ramp K_ω during this speed rampup stage with a constant q^*-axis current. It may be observed from (15) that for a system with a high inertia and high load torque during the startup period, the speed ramp ratio should be small. If a high acceleration K_ω is desired, the reference current i_q^* set in the synchronous rotating reference frame should be increased.

B. Constant Speed Reference With Decreasing q^*-Axis Current

The purpose of the previous stage is to accelerate the motor to a certain speed to allow the back-EMF signal to be sensed accurately. As discussed previously, it is preferred that the synchronous frame q^*-axis current be maintained at a larger value than the needed current component on the rotor q-axis, which is the current that the FOC will try to achieve ($i_q^* > i_q$). If it is suddenly switched to the back-EMF-based sensorless FOC scheme without any transition period, due to the mismatch of the current amplitudes, high current and torque ripple may then appear (see Fig. 5). The position estimation method presented in Section II has an open-loop structure. Inaccurate machine parameters, e.g., due to measurement errors, will affect the accuracy of the estimated rotor position. Additionally, in the speed rampup acceleration stage, the synchronous frame q^*-axis is lagging the rotor q-axis, resulting in a positive d-axis current component. This d-axis current produces a flux component that enhances the rotor PM flux, which may potentially increase the saturation level of the machine iron core and cause machine parameters to change. This phenomenon was observed experimentally in [21] for a similar SPMSM machine. The dependency of machine parameters on the saturation level depends on machine types and machine characteristics [21], [22], [25] and is hard to predict. Therefore, a transient period that makes the current amplitudes and consequently the saturation level of the machine to be in a close match before and after switching to the FOC mode is necessary.

A simple way to offer a smooth transition is to keep the speed constant while reducing the synchronous frame q^*-axis current. This is because, as may be observed from Fig. 2, when the

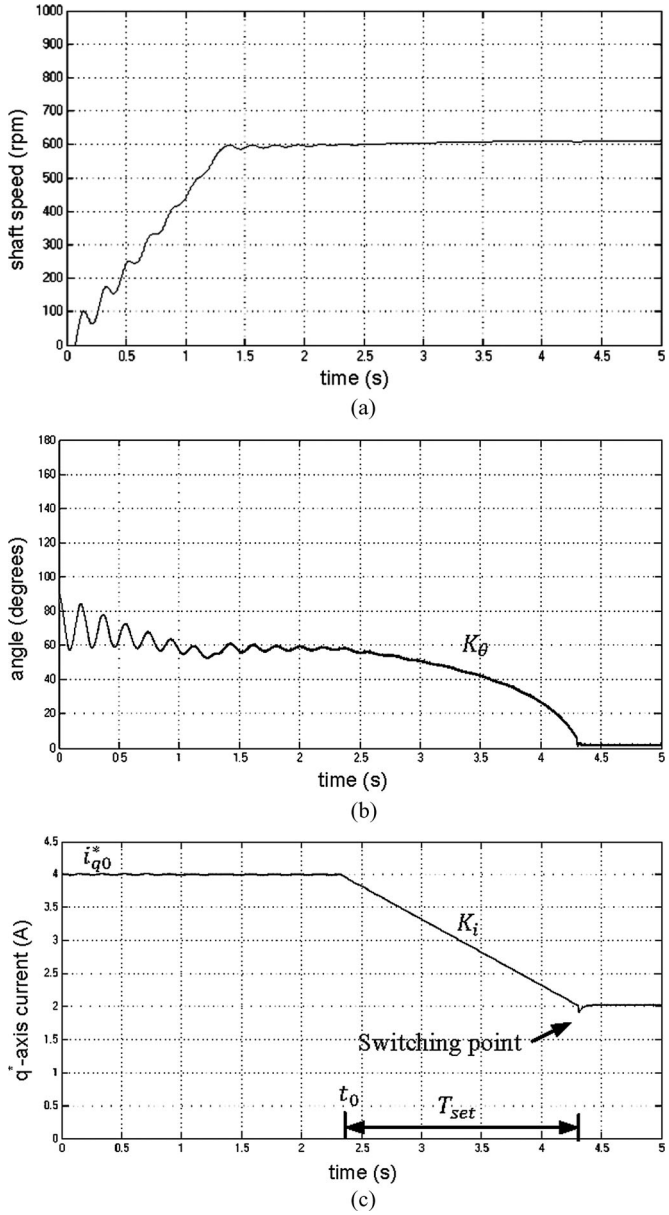

Fig. 3. Simulation results of the startup process. (a) Motor shaft speed during startup. (b) Transient behavior of angle θ_L. (c) Synchronous frame current i_q^* during startup.

synchronous frame q^*-axis current (i_q^*) is reduced in order to generate the same torque as before and balance the load torque, angle θ_L is forced to be reduced. The synchronous frame q^*-axis will then rotate toward the rotor q-axis. The current will approach to the value that will be generated in the FOC mode, and the rotor d-axis current component reduces to zero. The current and torque ripples during the switching to the FOC mode will then be reduced. The performance obtained from simulation of this startup process and the transition to the FOC mode is demonstrated in Fig. 3. The motor parameters are given in Section IV. The simulation results are achieved by solving the nonlinear equations (7)–(10) numerically using MATLAB.

During the speed rampup stage, oscillations of angle θ_L may be observed from Fig. 3(b). This indicates the self-stabilizing mechanism, as discussed previously. The speed rampup ratio K_ω used in this simulation is 89.5 rad/s^2. The load torque used in the simulation is known. Based on the result shown in Fig. 3(b), the average value for angle θ_L is found to be 65° in the acceleration period. By substituting this value into (14), the speed rampup ratio K_ω obtained is 91.1 rad/s^2, which is very close to the real K_ω value used. This validates the analytical (14), which is used for selecting a proper speed rampup ratio K_ω during the design stage.

As shown in Fig. 3(a), after the rotor speed has reached a desired value, the rotor speed is maintained constant by setting a constant speed reference command. The synchronous frame q^*-axis current is then decreased and the angle θ_L is forced to be reduced to zero correspondingly. A small threshold value for the angle θ_L may be set to control the instant when the FOC scheme should be switched in and take over the control. In this simulation, the threshold value of angle θ_L is set to be 5 electrical degrees and the FOC takes over the control at 4.3 s. Very small current ripple during this switching transient may be observed from Fig. 3(c).

In the current reducing transition period, an important parameter to set is the current reducing ratio K_i. The determination of this ratio is analyzed in the following.

The current profile in this transition period may be expressed as follows:

$$i_q^*(t) = i_{q0}^* - K_i(t - t_0) \tag{16}$$

where $t_0 \le t \le t_0 + T_{\rm set}$, and $i_{q0}^*, T_{\rm set}$ are defined as shown in Fig. 3(c).

As discussed previously, when the synchronous frame q^*-axis current i_q^* is decreasing, the angle θ_L will be reduced correspondingly in order to produce a torque that will balance the load torque. Therefore, it may be assumed that during the current decreasing transition period, the rotor speed does not change. This may be observed from Fig. 3(a). Therefore, by integrating (9), it is obtained that

$$\int_{t_0}^{t_0+T_{\rm set}} T_e(t)dt - \int_{t_0}^{t_0+T_{\rm set}} T_L(t)dt = J(\Omega_r(t_0+T_{\rm set}) - \Omega_r(t_0)) = 0. \tag{17}$$

Supposing the load torque does not change during this current decreasing period, its value will be equal to the motor torque at time t_0; therefore, $T_{L(t_0)} = K_T \cdot i_{q0}^* \cos(\theta_{L(t_0)})$. By substituting (7) into (17), the following is derived:

$$\int_{t_0}^{t_0+T_{\rm set}} i_q^*(t)\cos(\theta_L(t))dt = i_{q0}^* \cos(\theta_{L(t_0)})T_{\rm set} \tag{18}$$

where $i_q^*(t)$ is determined by (16), and angle $\theta_L(t)$ may be assumed to decrease linearly from its initial value $\theta_L(t_0)$ to zero as follows:

$$\theta_L(t) = \theta_L(t_0) - \frac{\theta_L(t_0)}{T_{\rm set}}(t - t_0). \tag{19}$$

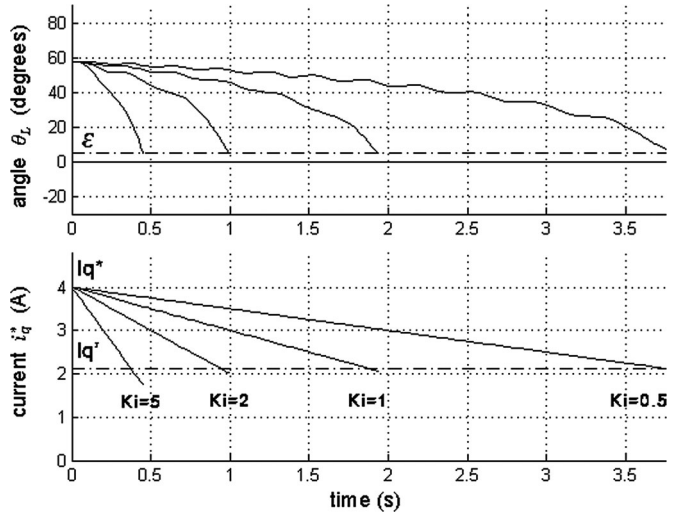

Fig. 4. Response of angle θ_L in relation to the variation of the synchronous frame q^*-axis current i_q^*.

By substituting (16), (19) into (18) and performing the integration in (18), it is obtained that

$$K_i = i_{q0}^* \frac{\theta_{L(t_0)} \cos(\theta_{L(t_0)}) - \sin(\theta_{L(t_0)})}{\cos(\theta_{L(t_0)})} K_\theta \qquad (20)$$

where K_θ describes how fast the angle θ_L reduces to zero, and is defined to be $\theta_{L(t_0)}/T_{\rm set}$.

Equation (20) shows that for a fixed initial angle $\theta_{L(t_0)}$, and fixed synchronous frame q^*-axis current i_{q0}^*, if the current decreasing ratio K_i is increased, a faster decrease of the angle $\theta_L(t)$ will be achieved. This may be observed from Fig. 4, where the behavior of angle $\theta_L(t)$ for different transient q^*-axis current profiles is shown. The results are obtained from the simulation model discussed previously.

When the angle $\theta_L(t)$ has reached the threshold value (5° in this case), the control is switched to the FOC mode. The q-axis current that will be maintained by the FOC is 2 A, as may be observed from Fig. 3(c). As shown in Fig. 4, for a large range of K_i (from 0.5 to 2), when angle $\theta_L(t)$ is reduced to the threshold value, the synchronous frame q^*-axis current is reduced to a value that is very close to 2 A, which ensures that very small current and torque ripple will occur if the FOC is switched in at this instant. But if K_i is too large and the current reduces too fast, when angle $\theta_L(t)$ is reduced to the threshold value, the synchronous frame q^*-axis current will be less than the desired current of 2 A, e.g., for case $K_i = 5$. A mismatch of the current amplitudes at the switching instant will increase the current and torque ripples. This ripple may be clearly observed in the experimental result shown in Fig. 5, where $K_i = 15$.

Equation (20) may be used to obtain a rough estimation of the desired current decreasing ratio K_i. By selecting a certain value for the angle $\theta_L(t)$ decreasing ratio K_θ, the current decreasing ratio K_i may be estimated using (20), and the current value at the switching instant $t_0 + T_{\rm set}$ may then be estimated by using (16). This current value should be close to $i_{q0}^* \cos(\theta_L(t_0))$, which is 2 A in this case. By following this method, it is found that

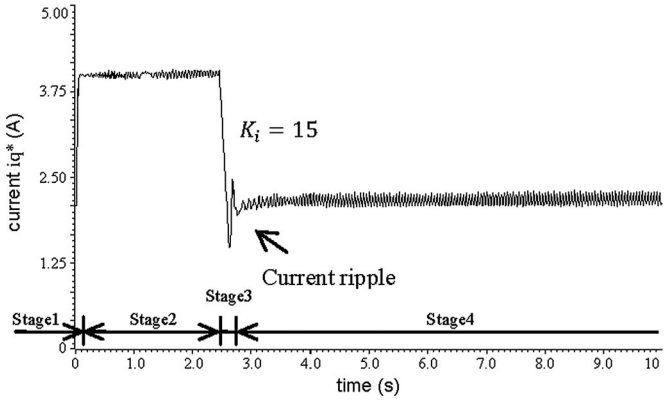

Fig. 5. Current ripples caused by setting a large decreasing ratio of synchronous frame q^*-axis current when switching from the startup stage to the FOC mode, i.e., from Stage 3 to Stage 4.

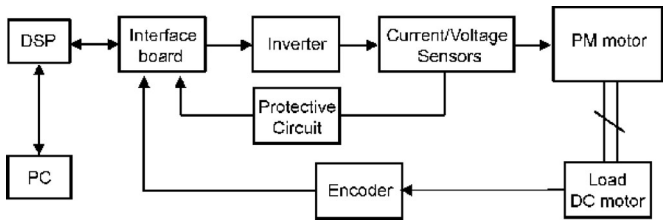

Fig. 6. Experimental hardware flowchart.

$K_i < 3.9$, which gives a relatively good indication as compared to the results shown in Fig. 4.

In summary, the startup strategy may be divided into the following four stages, as indicated in Fig. 5.

Stage 1: Rotor position initialization. By injecting dc currents or by initial rotor position detection based on magnetic saliency.

Stage 2: Speed rampup with constant current regulation. A constant current reference is given on the $q*$-axis of the synchronous reference frame. The speed is determined by a speed ramp command.

Stage 3: In this stage, the speed is held constant and the synchronous reference frame $q*$-axis current decreases to ensure an accurate estimation of the rotor position and a smooth transition to the FOC mode.

Stage 4: Switching and FOC mode operation. FOC is switched in at the end of Stage 3, when the estimated rotor position is accurate enough. The FOC takes over the control and the q-axis current command i_q is then determined by the speed control loop to further regulate the rotor speed.

IV. Test Platform and Experimental Results

The startup strategy discussed previously is tested using an experimental drive system. The experimental system consists of an SPMSM, a dc motor as the load, an eZdsp-F28335 controller, a Danfoss FC302 Series inverter, a 2048-pulses incremental encoder used for validating the rotor position estimation, and the CCS3.3 platform [26], [27]. The system topology is shown in Figs. 6 and 7. The parameters of the PM motor are given in Table I.

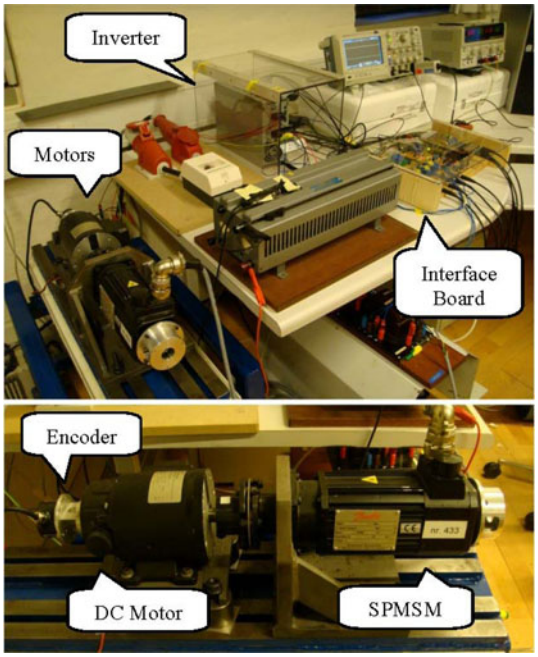

Fig. 7. Experimental platform.

TABLE I
MOTOR PARAMETERS

Surface Mounted PMSM			
Rated power	470 W	Stator resistance	2.35 Ω
Max. phase voltage	380 V	d-axis inductance	10 mH
Rated current	2.9 A	q-axis inductance	15.4 mH
Rated speed	2850 rpm	Permanent-magnet flux	0.132 Wb
Rated frequency	95 Hz	Inertia	3×10^{-3} kg·m^2
Rated torque	1.58 N·m	Pole pairs	2

In the experiment, the dc motor serves as the load. The switching from the startup strategy to the FOC strategy is performed at the speed of 20 Hz/600 r/min, which is around 20% of the rated speed. This is the minimum speed for most pump and fan applications. At this speed, the position estimated based on the back-EMF will be accurate enough. The startup performance of the PM motor drive system is demonstrated in Fig. 8, with the dc-motor acting as a load, and in Fig. 9, with the dc-motor open circuit (no load).

It is important to point out that in application, when switching from the startup stage to the FOC stage, a sudden jump of q-axis reference current i_q may occur, if the initial value of the integration block in the speed loop PI controller is not properly set. A proper initial value for this integrator could be the current value estimated from (16) as $i_q^*(t_0 + T_{\rm set})$.

A. Startup From Standstill to 600 r/min, With DC Motor Loaded

B. Startup From Standstill to 600 r/min, With DC-Motor Open Circuited (No Load)

It may be observed from Figs. 8(a) and 9(a) that in both loaded and non-loaded situations, the motor is able to be successfully accelerated to the desired speed. The reference current command set on the q^*-axis of the synchronous rotating reference frame

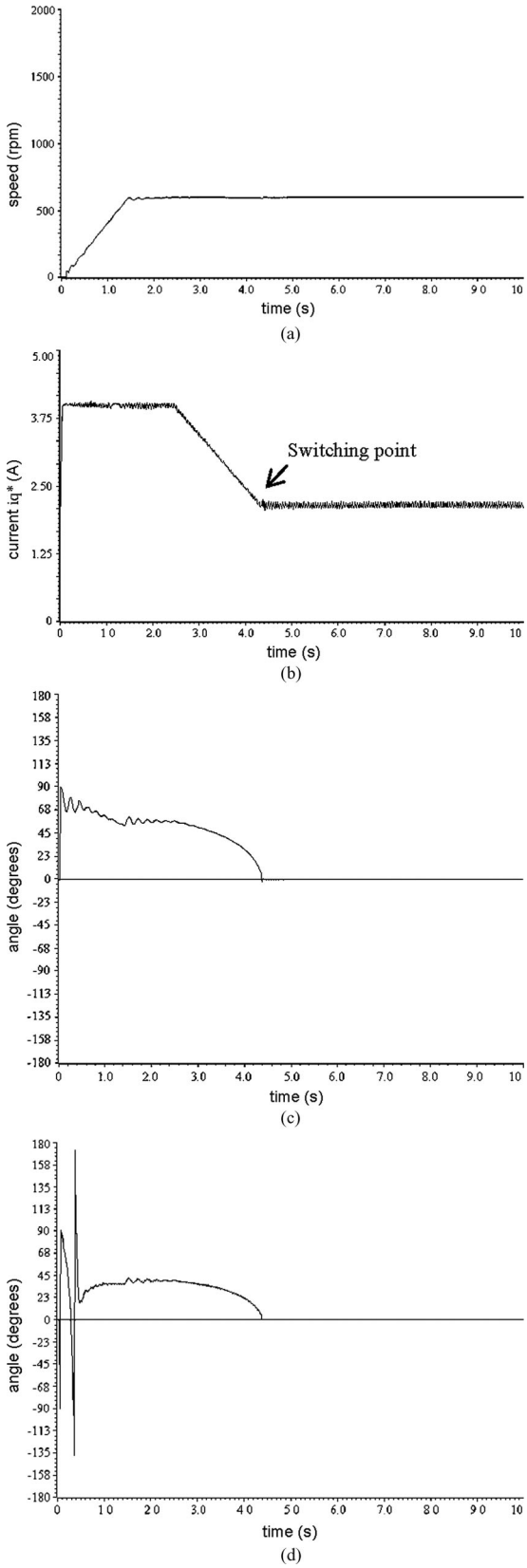

Fig. 8. Speed, current, and position behaviors in the startup stage with the dc motor loaded. (a) Rotor speed during startup. (b) Current iq^* during startup. (c) Transient behavior of angle θ_L, which is the angle between the synchronous rotating $q*$-axis and the real rotor q-axis measured by the encoder. (d) Transient behavior of angle θ'_L, which is the angle between the synchronous rotating $q*$-axis and the estimated rotor q-axis based on the back EMF.

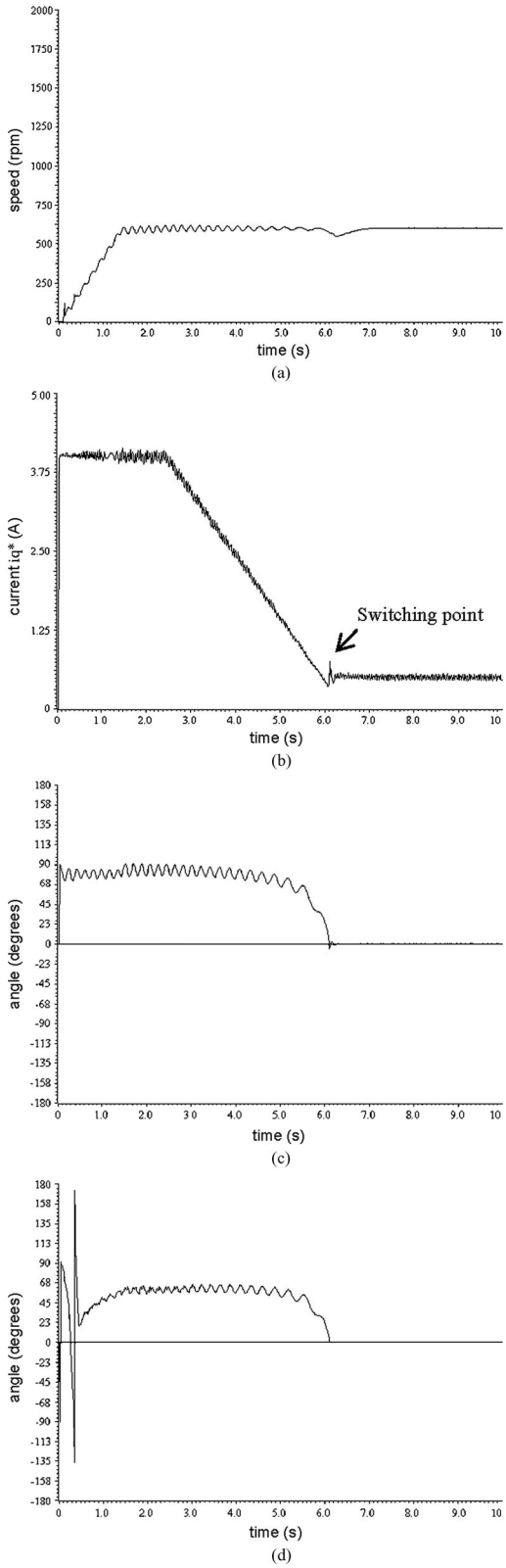

Fig. 9. Speed, current, and position behaviors in the startup stage with the dc motor open circuited (no load). (a) Rotor speed during startup. (b) Current iq^* during startup. (c) Transient behavior of angle θ_L, which is the angle between the synchronous rotating q^*-axis and the real rotor q-axis measured by the encoder. (d) Transient behavior of angle θ'_L, which is the angle between the synchronous rotating q^*-axis and the estimated rotor q-axis based on the back EMF.

is the same for both cases. In the loaded situation, the torque provided by the dc motor is proportional to the speed. The torque available from the dc motor is approximately 0.8 Nm at 600 r/min, as may be estimated from the steady-state q^*-axis current shown in Fig. 8(b). The sensorless FOC is switched in at 4.3 s for case A and at 6.0 s for case B. The difference in time is caused by the different load situations. The current ripple and hence the torque ripple during the transition period from the startup stage to the sensorless FOC stage is very small, as may be observed from Figs. 8(b) and 9(b).

The angle θ_L shown in Figs. 8(c) and 9(c) is the angle between the synchronous rotating frame q^*-axis and the real rotor q-axis. In applications, the real rotor position is actually unknown so that θ_L cannot be used directly, but it could be estimated. The angle between the synchronous rotating frame q^*-axis and the estimated rotor q-axis from the back-EMF-based sensorless method, which is denoted as θ'_L, is plotted in Figs. 8(d) and 9(d). The value of angle θ'_L, compared to a threshold value, is used to control the instant when the sensorless FOC should be switched in, as mentioned previously. It may be observed from these figures that the position estimated from the back-EMF is not stable at low speed. It is of further interest to observe that even at a reasonably high speed, before introducing the current reducing transition period, the estimated position is still not accurate. This may be observed by comparing Fig. 8(c) versus (d), and Fig. 9(c) versus (d). This position error is caused by inaccurate machine parameters that affect the estimated rotor position, as discussed in Section III-B. During the current decreasing period, since the d-axis current component is reduced, the angle θ'_L approaches to the angle θ_L, and both of them finally reduce to zero. At the same time the synchronous frame q^*-axis current approaches to the real q-axis current. Hence, switching from the startup stage to the sensorless FOC stage becomes very smooth.

In the results presented in Fig. 9 where the dc motor is open circuited (no load), smaller rising time and larger speed ripple may be observed, as the net torque used for accelerating the motor becomes larger, causing higher oscillation of the speed. However, this oscillation could be reduced by reducing the speed acceleration ramp ratio K_ω.

V. Conclusion

The advantages of the new current regulation startup strategy are that the stator current is under control and it has a self-stabilization mechanism even with no speed information feedback. It can work with different load conditions, and it is dynamically stable under a proper setting of the reference current command and the speed rampup ratio according to the load and system parameters. A new transition process is introduced before switching from the startup strategy to the sensorless FOC strategy. This transition period guarantees that the position estimated from the back-EMF-based sensorless algorithm is accurate. The synchronous rotating frame q^*-axis current component in the startup stage may be automatically adjusted to the value that will be generated in the FOC stage, and the d-axis current component will be eliminated. This ensures very small current and torque ripple during the transition from the startup stage to

the sensorless FOC stage. Detailed analysis and design guides for the current regulation startup strategy are also given and are validated using simulation and experimental results.

REFERENCES

[1] R. Dhaouadi, N. Mohan, and L. Norum, "Design and implementation of an extended Kalman filter for the state estimation of a permanent magnet synchronous motor," *IEEE Trans. Power Electron.*, vol. 6, no. 3, pp. 491–497, Jul. 1991.

[2] S. Bolognani, M. Zigliotto, and M. Zordan, "Extended-range PMSM sensorless speed drive based on stochastic filtering," *IEEE Trans. Power Electron.*, vol. 16, no. 1, pp. 110–117, Jan. 2001.

[3] Y. A.-R. I. Mohamed, "Design and implementation of a robust current-control scheme for a PMSM vector drive with a simple adaptive disturbance observer," *IEEE Trans. Ind. Electron.*, vol. 54, no. 4, pp. 1981–1988, Aug. 2007.

[4] J. Lee, J. Hong, K. Nam, R. Ortega, L. Praly, and A. Astolfi, "Sensorless control of surface-mount permanent-magnet synchronous motors based on a nonlinear observer," *IEEE Trans. Power Electron.*, vol. 25, no. 2, pp. 290–297, Feb. 2010.

[5] C. Y. Wang and L. Y. Xu, "A novel approach for sensorless control of PM machines down to zero speed without signal injection or special PWM technique," *IEEE Trans. Power Electron.*, vol. 19, no. 6, pp. 1601–1607, Nov. 2004.

[6] J. S. Kim and S. K. Sul, "New approach for high-performance PMSM drives without rotational position sensors," *IEEE Trans. Power Electron.*, vol. 12, no. 5, pp. 904–911, Sep. 1997.

[7] B. K. Bose, "Power electronics and motor drives—Recent progress and perspective," *IEEE Trans. Ind. Electron.*, vol. 56, no. 2, pp. 581–588, Feb. 2009.

[8] A. Consoli, G. Scarcella, and A. Testa, "Industry application of zero-speed sensorless control techniques for PM synchronous motors," *IEEE Trans. Ind. Appl.*, vol. 37, no. 2, pp. 513–521, Mar./Apr. 2001.

[9] B. H. Kenny and P. E. Kascak, "Sensorless control of permanent magnet machine for NASA flywheel technology development," NASA, Washington, DC, Tech. Rep. TM-2002-211726, Jul. 2002.

[10] H. W. De Kock, M. J. Kamper, and R. M. Kennel, "Anisotropy comparison of reluctance and PM synchronous machines for position sensorless control using HF carrier injection," *IEEE Trans. Power Electron.*, vol. 24, no. 8, pp. 1905–1913, Aug. 2009.

[11] G. Ahmad and H. Tsuyoshi, "Very low speed sensorless vector control of synchronous reluctance motors with a novel startup scheme," in *Proc. 22nd Annual IEEE Appl. Power Electron. Conf.*, 2007, pp. 396–402.

[12] S. Ogasawara and H. Akagi, "An approach to real-time position estimation at zero and low speed for a PM motor based on saliency," *IEEE Trans. Ind. Appl.*, vol. 34, no. 1, pp. 163–168, Jan./Feb. 1998.

[13] Y. Jeong, R. D. Lorenz, T. M. Jahns, and S. Sul, "Initial rotor position estimation of an interior permanent-magnet synchronous machine using carrier-frequency injection methods," *IEEE Trans. Ind. Appl.*, vol. 41, no. 1, pp. 38–45, Jan./Feb. 2005.

[14] R. S. Wu and G. R. Slemon, "A permanent magnet motor drive without a shaft sensor," *IEEE Trans. Ind. Appl.*, vol. 21, no. 5, pp. 1005–1011, Sep./Oct. 1991.

[15] N. Chen, Z. Wang, S. Yu, W. Gui, and Y. Guo, "A new starting method of sensorless PMSM motors based on STM32F103B," in *Proc. 29th Chinese Control Conf.*, 2010, pp. 4964–4968.

[16] F. Genduso, R. Miceli, C. Rando, and G. R. Galluzzo, "Back EMF sensorless-control algorithm for high-dynamic performance PMSM," *IEEE Trans. Ind. Electron.*, vol. 57, no. 6, pp. 2092–2100, Jun. 2010.

[17] M. Fatu, R. Teodorescu, I. Boldea, and G. D. Andreescu, "I-F starting method with smooth transition to EMF based motion-sensorless vector control of PM synchronous motor/generator," in in *Conf. Rec. Power Electron. Spec. Conf.*, 2008, pp. 1481–1487.

[18] A. Stirban, I. Boldea, G.-D. Andreescu, D. Iles, and F. Blaabjerg, "Motion sensorless control of BLDC PM motor with offline FEM info assisted state observer," in *12th Int. Conf. OPTIM*, 2010, pp. 321–328.

[19] J. Holtz and J. T. Quan, "Drift and parameter compensated flux estimator for persistent zero stator frequency operation of sensorless controlled induction motors," *IEEE Trans. Ind. Appl.*, vol. 39, no. 4, pp. 1052–1060, Jul./Aug. 2003.

[20] B. N. Mobarakeh, F. Meibody-Tabar, and F.-M. Sargos, "Back-EMF estimation based sensorless control of PMSM: Robustness with respect to measurement errors and inverter irregularities," in *Conf. Rec. 39th IEEE IAS Annu. Meet.*, 2004, vol. 3, pp. 1858–1865.

[21] K. Y. Lu, M. Vetuschi, P. O. Rasmussen, and A. E. Ritchie, "Determination of high-frequency d- and q-axis inductances for surface-mounted permanent-magnet synchronous machines," *IEEE Trans. Instrum. Meas.*, vol. 59, no. 9, pp. 2376–2382, Sep. 2010.

[22] Z. Q. Zhu, Y. Li, D. Howe, C. M. Bingham, and D. Stone, "Influence of machine topology and cross-coupling magnetic saturation on rotor position estimation accuracy in extended back-EMF based sensorless PM brushless AC drives," in *Proc. 42nd IAS Annu. Meet.*, 2007, pp. 2378–2385.

[23] M. Boussak, "Implementation and experimental investigation of sensorless speed control with initial rotor position estimation for interior permanent magnet synchronous motor drive," *IEEE Trans. Power Electron.*, vol. 20, no. 6, pp. 1413–1422, Nov. 2005.

[24] F. Andoh, "Moment of inertia identification using the time average of the product of torque reference input and motor position," *IEEE Trans. Power Electron.*, vol. 22, no. 6, pp. 2534–2542, Nov. 2007.

[25] P. Guglielmi, M. Pastorelli, and A. Vagati, "Cross-saturation effects in IPM motors and related impact on sensorless control," *IEEE Trans. Ind. Appl.*, vol. 42, no. 6, pp. 1516–1522, Nov./Dec. 2006.

[26] *TMS320F28335 Digital Signal Controllers Data Manual,* Texas Instruments, Dallas, Literature Number SPRS439 F, Jun. 2007–Apr. 2009.

[27] *Code Composer Studio User's Guide,* Texas Instruments, Dallas, Literature Number SPRU328B, Feb. 2000.

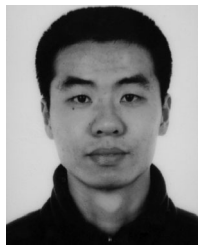

Zihui Wang (S'07) received the B.S. degree in electrical engineering from Zhejiang University, Hangzhou, China, in 2007, where he is currently working toward the Ph.D. degree.

From 2009 to 2010, he was a Research Assistant in the University of Aalborg, Aalborg, Denmark. His current research interests include control of power electronic systems and control of permanent magnet synchronous machines with sensorless algorithms.

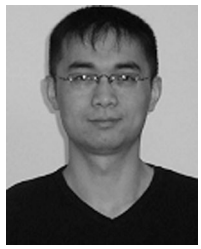

Kaiyuan Lu received the B.S. and M.S. degrees from Zhejiang University, Zhejiang, China, in 1997 and 2000, respectively, and the Ph.D. degree from Aalborg University, Aalborg, Denmark, in 2005.

In 2005, he became an Assistant Professor in the Department of Energy Technology, Aalborg University, where he has been an Associate Professor since 2008. His research interests include design of permanent magnet machines, finite-element method analysis, and control of permanent magnet machines.

Frede Blaabjerg (S'86–M'88–SM'97–F'03) received the Ph.D. degree from Aalborg University, Aalborg, Denmark, in 1992.

From 1987 to 1988, he was with ABB-Scandia, Randers. In 1992, he joined Aalborg University as an Assistant Professor. He was then promoted to Associate Professor in 1996 and then Full Professor in power electronics and drives in 1998. He has been a part-time research programme leader in wind turbines at Research Center Risoe, Roskilde, Denmark. From 2006 to 2010, he served as Dean of the faculty of Engineering, Science and Medicine, Aalborg University. In 2009, he was a Visiting Professor at Zhejiang University, Hangzhou, China. His research interests include power electronics and its applications like wind turbines, photovoltaic systems, and adjustable speed drives.

Dr. Blaabjerg has been the Editor-in-Chief of the IEEE TRANSACTIONS ON POWER ELECTRONICS since 2006. From 2005 to 2007, he was a Distinguished Lecturer for the IEEE Power Electronics Society, and from 2010 to 2011, a Distinguished Lecturer of the IEEE Industry Applications Society. He received the 1995 Angelos Award for his contribution in modulation technique and the Annual Teacher prize at Aalborg University in 1995. In 1998, he received the Outstanding Young Power Electronics Engineer Award from the IEEE Power Electronics Society. He has received ten IEEE Prize paper awards and another prize paper award at the Power Electronics and Intelligent Control for Energy Conservation Conference, Warsaw, Poland, in 2005. He received the IEEE Power Electronics Society Distinguished Service Award in 2009 as well as the European Power Electronics and Drives Association Power Electronics and Motion Control Conference (EPE-PEMC) 2010 Council award.